Reliability Analysis of 15MW Horizontal Axis Wind Turbine Rotor Blades Using Fluid-Structure Interaction Simulation and Adaptive Kriging Model

Arvind Keprate[a], Nikhil Bagalkot[b], Muhammad Salman Siddiqui[c], Subhamoy Sen[d]

[a] Department of Mechanical, Electronics, and Chemical Engineering, Oslo Metropolitan University, 0166 Oslo, Norway
[b] TechnipFMC, Lysaker, Norway
[c] Department of Mechanical Engineering and Technology Management, NMBU, Ås, Norway
[d] School of Civil and Environmental Engineering, IIT Mandi, India

Abstract:
Over the course of the last four decades, the rotor diameter of Horizontal Axis Wind Turbines (HAWTs) has undergone a substantial increase, expanding from 15 meters (30kW) to an impressive 240 meters (15MW), primarily aimed at enhancing their power generation capacity. This growth in blade swept area, however, gives rise to heightened loads, stresses and deflections, imposing more rigorous demands on the structural robustness of these components. To prevent sudden failure and to plan effective inspection, maintenance, and repair activities, it is vital to estimate the reliability of the rotor blades by considering all the forces (aerodynamic and structural dynamics) acting on them over the turbine's lifespan. This research proposes a comprehensive methodology that seamlessly combines fluid-structure interaction (FSI) simulation, Kriging model/algorithm and Adaptive Kriging Monte Carlo Simulation (AKMCS) to assess the reliability of the HAWT rotor blades. Firstly, high-fidelity FSI simulations are performed to investigate the dynamic response of the rotor blade under varying wind conditions. Recognizing the computationally intensive nature and time-consuming aspects of FSI simulations, a judicious approach involves harnessing an economical Kriging model as a surrogate. This surrogate model adeptly predicts blade deflection along its length, utilizing training and testing data derived from FSI simulations. Impressively, the Kriging model predicts blade deflection 400 times faster than the FSI simulations, showcasing its enhanced efficiency. The optimized surrogate model is then used to estimate the flap wise blade tip deflection for one million wind speed samples generated using Weibull distribution. Thereafter, to evaluate the reliability of the blades, statistical modeling using methods such as Monte Carlo Simulation (MCS), AKMCS is performed. The results demonstrate the faster convergence of AKMCS requiring only 21 samples, as opposed to 1 million samples for MCS with minimal reduction in the precision of the estimated probability of failure (P_f) and reliability index (β). Demonstrated on the backdrop of an IEA-15MW offshore reference WT rotor blade, the proposed methodology underscores its potential to be seamlessly incorporated into the creation of WT digital twins, due to its near real-time predictive capabilities for P_f and β assessments.

1. Introduction

The need of boosting alternative renewable energy sources to reduce the dependency on conventional fossil fuel dependency has become an important global issue [1]. It is forecasted that 30% of the global electricity production will come from wind energy by 2050, with 12% from offshore wind and 18% from onshore wind, thus wind energy becoming a 'new conventional' rather than a non-conventional energy resource [2]. Industry experts predict that in the coming years U.S., China, and some of the European Union countries have planned to increase the contribution of the wind energy share to their energy demand to about 20% [3]. The increased

reliance on wind energy has pushed engineers to build wind turbines (WTs) to produce more power output by increasing the blade size (and consequently increasing the blade swept area) [4]. Significant progress has been made over the last four decades, as the WT generation capacity has increased, from kW-class to MW class. The increase in capacity is credited to a significant increase in the rotor diameter from approximately 30m (kW) to 240m (15MW) recently [5]. However, increasing size and flexibility of large wind turbine blades, makes them more prone to aeroelastic issues emanating by fluid-structure interaction (FSI). The resulting aeroelastic effects on rotor blades may augment the risk of instabilities from blade deflection, vibration, and flutter during the operation of WTs [6]. In addition, due to their increasingly thin shape, WT blades grow more vulnerable to deflections and material fatigue. Furthermore, the problem becomes critical when WTs operate in a wind farm under the wake distribution of other WTs, thereby leading to uneven distribution of loads on the blades, further pushing the blade towards failure. Therefore, for optimizing WT design, maintaining structural integrity, and maximizing energy output, understanding and minimizing aeroelastic effects is essential by precisely modeling the FSI on the rotor blades. An FSI model integrates the aerodynamic forces acting on the rotor blades with their structural behavior by accounting for the complex coupling between aerodynamics and structural dynamics. Numerous methods have been developed to study the interaction of fluid and the WT rotor blade, of which the Blade Element Method (BEM) is widely applied, the validity [7, 8] along with the limitations of BEM is well discussed in the scientific literature [9, 10].

BEM theory was utilized to evaluate the aerodynamic performance of a horizontal axis wind turbine in work by Shen et al. (2014) [11]. The researchers discovered that BEM accurately predicted the WT's power output, thrust, and tip speed ratio compared to experimental data. The study proved that BEM might be utilized to predict performance in steady-state circumstances. Using BEM-based techniques, Shives and Schreck (2017) [12] investigated the impact of various rotor configurations on WT performance. Variable-pitch and fixed-pitch rotor designs, as well as their power output and loads, were all examined. The findings demonstrated that BEM successfully captured the trends and relative performance differences among the various rotor configurations, offering suggestions for improving WT design. In a different work by Barlas (2014) [13], the dynamic response of a WT under turbulent inflow conditions was examined using BEM theory. The researchers examined how turbulent wind affected the rotor blades' aeroelastic behavior. They discovered that BEM-based approaches could reasonably capture the dynamic response under moderately turbulent conditions. However, the precision fell highly turbulent flow conditions, highlighting the limitations of BEM in capturing unsteady aerodynamic effects. Gebraad et al. (2016) [14] investigated the effects of various control strategies on WT performance and power output using BEM theory in conjunction with optimization algorithms. The study showed the potential of BEM-based techniques for improving WT control settings to maximize energy capture while considering different restrictions. The findings gave important information about operating and designing WT for increased performance. Cheng et al. (2020) [15] examine the impact of blade twist distribution on the aerodynamic performance of a WT using BEM. They study the impact of various blade twist configurations on power generation and load. The outcomes showed that BEM-based techniques could correctly predict performance trends and the ideal twist distribution for increased energy extraction. BEM-based methods are computationally efficient and generally offer good estimates of the aeroelastic behavior of flexible blades [16], nevertheless, BEM theory is based on the one-dimensional momentum equilibrium and neglects the 3D effects which is vital to capture the entire aerodynamic phenomena accurately. Consequently, BEM approaches are still being improved and honed by researchers, to account for all complex unsteady,

and 3D aerodynamic effects frequently by integrating corrections and combining them with additional advanced computational tools to improve the accuracy of WT analysis and design [17]. One alternative to BEM in evaluating the blade structural response to fluid aerodynamics is a high-fidelity Fluid-Structure Interaction (FSI) model composed of a finite volume computational fluid dynamics (CFD) solver and a finite element method (FEM) solver, which can consider the coupling effect of aerodynamic and structural field, thus overcoming the limitations of the BEM method [18]. Therefore, over last decade there has been surge in the usage of CFD to understand the FSI of the air and blade [19-21]. The developments in CFD and FSI for the application of WT blades is well documented [22, 23]. However, computational FSI is not cheap and has its own share of difficulties, like the results are over dependent on the grid/mesh size, and the type of turbulence model [21]. This is in addition to the large requirement of computing power needed, especially when working on a large wind farm. Thus, FSI simulations' accuracy comes with mounting computational costs and time, particularly for complex model and flow physics seen in WT blades [21]. This leads to a compromise between accuracy and cost of computing.

A well-known approach to overcome this shortcoming is the use of machine learning (ML) based surrogate models (SMs) [24]. For instance, Zhou at al [25] combined delayed proper orthogonal decomposition (d-POD) with long short-term memory (LSTM) network to predict the unsteady wind turbine wake velocity. Likewise, Wilson and Wakes [26] used a SM (linear regression, random forest) in combination with CFD simulation to study and predict the wake effect in an offshore wind farm. Richmond, and Sobey [27] used five different ML algorithms along with the CFD approach to predict the flow field around wind turbine. Bagalkot et al [28] employed Gradient Boosting Regressor coupled with CFD simulations to predict the force distribution over a 5MW wind turbine blade. Morato, et al [29], developed a Kriging based framework to evaluate the reliability of the support structure of the NREL 5MW WT model. To the best of our knowledge there are only handful of studies that employ ML based SMs to understand the response of rotor blade to air flow around it. None, of the studies, uses structural response (such as stress, displacement etc.) obtained from the SM-FSI simulation to estimate the reliability of the rotor blades.

The main objective of this study is to formulate and validate a 2-step methodology, leveraging the Kriging algorithm, for conducting an exhaustive reliability analysis of the rotor blades of the IEA-15MW [30] offshore reference WT. This entails utilizing the Kriging algorithm as a SM for FSI simulations and adaptively training it during reliability analysis, aiming to establish it as a computationally efficient and accurate alternative to conventional Monte Carlo Sampling (MCS) methods. This study seeks to not only enhance the computational efficacy and precision in reliability analysis but also to bridge a notable research gap concerning the IEA-15MW reference turbine. The novelty of this research is that it employs Kriging algorithm not only as a SM for FSI simulation but also, by adaptively training it during reliability analysis, the model can be used as an alternative to MCS methods, thus converging faster with minimal drop in accuracy. Moreover, the application of Kriging algorithm as a SM for predicting blade deflection exhibits the potential for substantial computational time savings (400 times faster) compared to conventional FSI simulations.

The subsequent sections of the paper are organized as follows: Section 2 comprehensively outlines the proposed methodology for conducting reliability analysis on the WT rotor blades. The operationalization of this methodology is vividly exemplified through a case study, expounded in Section 3. Section 4 extends the discourse by shedding light on potential future avenues of the

proposed methodology. Ultimately, Section 5 encapsulates the paper, drawing together significant findings and conclusions of this research.

2. Methodology

2.1 General

The flowchart of the proposed two-step methodology for evaluating the reliability of WT rotor blades is depicted in Figure 1. In the first step, a Kriging-based SM is trained using the dataset obtained from FSI simulations. The simulation was conducted for eight distinct wind speeds, specifically 3 m/s, 9 m/s, 11 m/s, 12.5 m/s, 15 m/s, 17.5 m/s, 21 m/s, and 25 m/s. Specifically, the simulation outcomes corresponding to wind speeds of 12.5 m/s and 17.5 m/s, were earmarked as test datasets, while the rest of dataset was used for training the Kriging model. To optimize the performance of the Kriging model, Bayesian optimization is employed to select the most suitable hyperparameters. The model's accuracy is then evaluated on the test dataset. This model is the used to estimate the deflection of the rotor blade caused by aerodynamic loads.
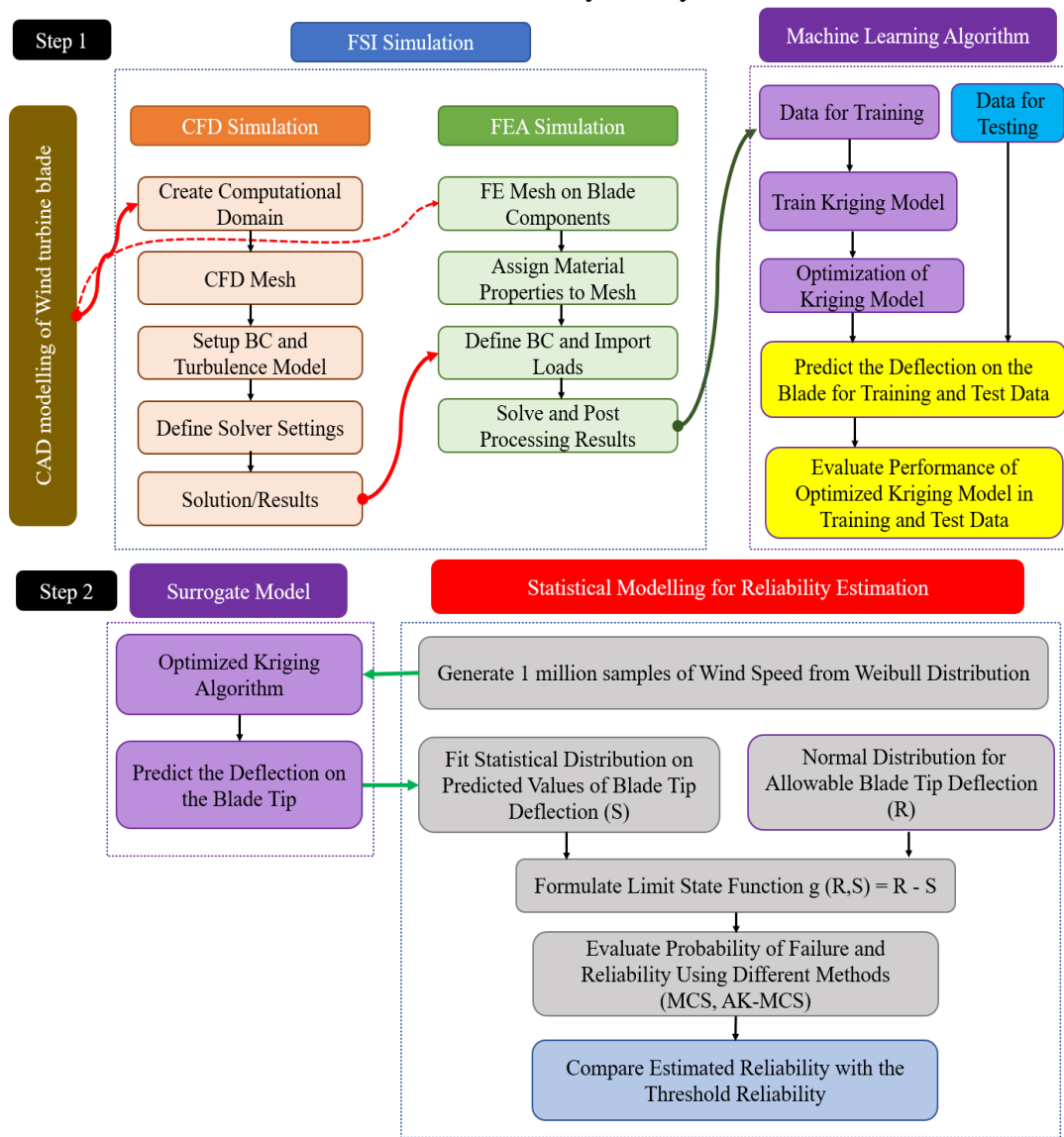

Figure 1: Schematic of the proposed methodology for performing reliability analysis of the rotor blade

Moving to the second step, the optimized Kriging model is utilized to predict blade tip deflection for one million samples of wind speed generated using the Weibull distribution [31]. Then, a limit state function for the variable blade tip deflection is formulated. The Probability of Failure (PoF) is initially estimated using the Monte Carlo Simulation (MCS) method. However, since MCS suffers from limitations such as high computational cost, slow convergence rate, and non-optimized sampling efficiency, we address these issues by employing the Adaptive Kriging Monte Carlo Sampling (AKMCS) approach. AKMCS adaptively updates the surrogate model and concentrates sampling efforts in critical regions. These enhancements make AKMCS a more efficient and effective method for uncertainty quantification and reliability analysis compared to traditional MCS. In the following subsections, we will provide a detailed explanation of each step of the methodology.

2.2 FSI Modeling

FSI methods for analyzing and solving fluid-structure interactions are categorized into two main types: the direct solution method and the load transfer method [32]. The direct solution method, exemplified by the Arbitrary Lagrangian-Eulerian (ALE) method, solves the FSI problem as a coupled system, simultaneously addressing the fluid and structure equations. This approach accounts for the interactions between the fluid and structure at each time step, resulting in precise predictions of their mutual influence. However, this method comes with drawbacks, including high computational cost and time consumption, particularly for large-scale and transient simulations. In contrast, the load transfer method treats the fluid and structure as separate entities, managing their interactions through a load transfer process (as depicted in Fig. 1). In this method, the fluid and structure domains are solved independently, and information related to forces and displacements is exchanged iteratively at the fluid-structure interface. This approach offers computational efficiency compared to the direct solution method, making it suitable for handling larger and more complex FSI simulations.

The main aim in the load transfer FSI modeling is to consider the coupling effect of fluid and solid by solving ,the equation of fluid region (Eq. 1 & 2) and structural region (Eq. 3) and finally to discover the interaction characteristics between the two. The equations governing the behavior of the fluid region are expressed in terms of the Navier-Stokes equations and can be written as:

$$\frac{\partial u_f}{\partial t} + (u_f \cdot \nabla)u_f = -\frac{1}{\rho_f \nabla p_f} + v_f \nabla_f^{2u} + f_f \quad \text{Eq. 1}$$

$$\nabla \cdot u_f = 0 \quad \text{Eq. 2}$$

where u_f is the fluid velocity vector, t is time, ρ_f is the fluid density, p_f is the fluid pressure, v_f is the fluid kinematic viscosity and f_f represents external force terms acting on the fluid such as body forces (e.g., gravity), surface forces (e.g., pressure or shear forces applied to the fluid boundary. Likewise, the equations for solid mechanics describe the structural behavior and can be written as:

$$\nabla \cdot u_s = \frac{\rho_s d_s^{2u}}{dt^2} = \nabla \cdot T_s + f_s \quad \text{Eq. 3}$$

where u_s is the solid displacement vector, ρ_s is the solid density, t is time, T_s is the stress tensor for the solid, f_s represents any external forces acting on the solid. To couple the fluid and solid

domains, interface conditions are imposed. These conditions ensure the conservation of fluid and structural parameters termed kinematic and dynamic conditions. The former condition enforces the equality of velocities at the fluid-solid interface and expressed as:

$$u_f = u_s \qquad \text{Eq. 4}$$

While the dynamic condition ensures that the fluid and solid forces at the interface are balanced, the stress or pressure at the interface between the fluid and the surface relates to each other. Thus, the coupling effect occurring in the contact region of the fluid and the solid must abide by the conservation of the fluid and structural parameters as shown in Eq. 4.

2.3 Kriging Model

Kriging model, also known as Gaussian process regression, is a stochastic interpolation technique, that has emerged as valuable tools in reliability analysis for engineering systems [33]. A Kriging model aims to construct a SM that captures the relationship between the input variables and the output. The model assumes that the output is a realization of a Gaussian process, defined by a mean function and a covariance function. The mean function represents the deterministic trend of the output. It is typically assumed to be a constant or a linear function of the input variables. The mean function can be expressed as [34]:

$$\mu(x) = \alpha_0 \, x_0 + \alpha_1 x_1 + \alpha_2 x_2 + \ldots + \alpha_p x_p \quad \text{Eq. 5}$$

where $\mu(x)$ is the mean function, α_0, α_1, α_2, ..., α_p are the regression coefficients, and x_1, x_2, ..., x_p are the input variables. The covariance function characterizes the spatial correlation between different points in the input space. It is usually defined based on the distance between the input points. Although there are many available covariance functions (also called kernel), the most commonly used one is the squared exponential function, given by:

$$k(x, x') = \sigma^2 \exp(- \|x - x'\|^2 / (2l^2)) \quad \text{Eq. 6}$$

where $k(x, x')$ is the covariance function between input points x and x', σ^2 is the variance parameter, l is the length scale parameter, and $\|x - x'\|^2$ represents the squared Euclidean distance between x and x'. Based on the mean function and covariance function, the SM can be expressed as:

$$Y(x) = \mu(x) + Z(x) \quad \text{Eq. 7}$$

where $Y(x)$ is the output variable, $\mu(x)$ is the mean function, and $Z(x)$ represents the random component, assumed to follow a Gaussian process with zero mean and covariance function $k(x, x')$. Using a training dataset with known input-output pairs, the regression coefficients (α) and hyperparameters (σ^2, l) are estimated through suitable optimization techniques. Once the suitable set of hyper-parameters are obtained, the optimized model is then used to predict the response variable.

2.4 Statistical Modeling for Reliability Estimation

The goal of reliability analysis is to assess a component's/system's failure probability while considering different sources of uncertainties. This is achieved by formulating a limit state function (also called as G function) by expressing the relationship between the input variables (e.g., loads,

material properties) and the system's response (e.g., stress, deflection). Mathematically, the G function can be defined as [35]:

$$G (R, S) = R - S \qquad \text{Eq. 8}$$

where R represents the system capacity variable (attributed to strength properties mostly) and S is the demand variable (attributed to loading). To estimate the reliability using the G function, a common approach is to determine the failure probability, denoted as P_f, which is the probability that $G (R, S) \leq 0$. Generally, evaluating G function requires analysis of sophisticated, computationally demanding numerical models, making the estimation of P_f a challenging task. The MCS method is the most widely used and established method for the reliability analysis [29]. This technique is probably the best option for reliability problems with explicit limit state functions which are 'easy' or 'cheap' to evaluate. However, it is computationally demanding, especially for problems with small P_f and time-consuming models. Consequently, researchers have resorted to various variance minimization techniques such as quasi MCS, importance sampling or subset simulations when higher accuracy is needed near the failure region. However, even these techniques are computationally demanding. Another faster approach for reliability analysis is analytical approaches such as First Order Reliability Method (FORM) or Second Order Reliability Method (SORM) which approximate the G function near the most probable point of failure [35]. Nevertheless, These methods are prone to large errors, especially when the G function is non-linear. In recent years several SM (such as Support Vector Machine [36], Polynomial Chaos Expansion [37], Kriging [29]) have been coupled with random simulation techniques (such as MCS) to significantly increase the efficiency of reliability analysis with minimal drop in the accuracy. In our proposed methodology we couple Adaptive Kriging model with MCS to estimate the P_f and the reliability index. In the subsequent section we demonstrate the applicability of the proposed methodology via a detailed case study.

3. Illustrative Case Study

3.1 Wind Turbine Rotor Blade CAD Model

In this case study we use the 15MW IEA Wind reference WT model jointly designed by National Renewable Energy Laboratory (NREL), University of Maine (UMaine) and the Technical University of Denmark (DTU). The reference wind turbine is a three-bladed horizontal-axis turbine, and its specific details can be found in the work by Gaertner et al. [30]. A synopsis of the main parameters of the reference WT is presented in Table 1.

Table 1: Blade Properties

Description	Value	Units
Power Rating	15	MW
Blade Length	117	m
Rotor Diameter	240	m
Root Diameter	5.20	m
Root Cylinder Length	2.34	m
Maximum Chord	5.77	m
Max Chord Position (Spanwise)	27.2	m
Tip Prebend	4.00	m
Precone	4.00	Degrees
Cut-in Wind Speed	3.00	m/s

Cut-out Wind Speed	25.0	m/s
Rated wind Speed	10.88	m/s
Minimum rotor speed	5	rpm
Maximum rotor speed	7.55	rpm
Rotor orientation	Upwind	
Control	Variable Speed and Pitch	
Number of blades	3	

Figure 2 illustrates the external profile of the rotor blade, highlighting the locations of various airfoil sections and the prebend. The blade has a length of 117 meters, a root diameter of 5.2 meters, and a maximum chord of 5.77 meters at approximately 20% span from the root.
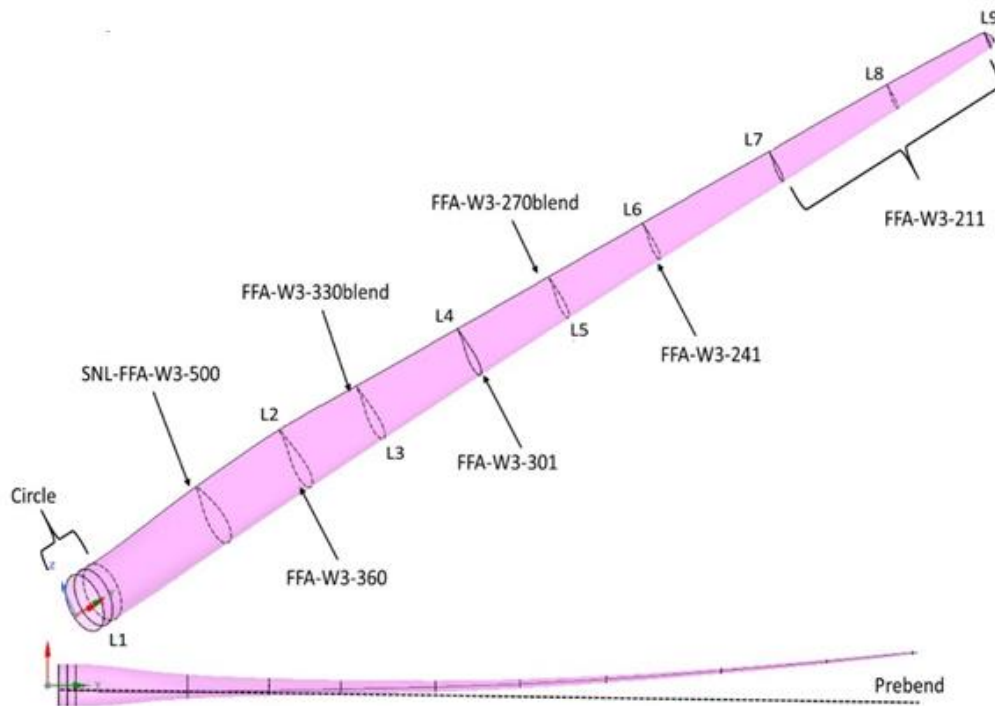
Figure 2: Outer profile of a single wind turbine blade, with clear indications of various airfoil sections

3.2 FSI Modeling
After creating the CAD model of the rotor blade, the first step is to perform the load transfer FSI modeling which involves performing CFD and FEA simulations. The next sub-section presents the details of the CFD flow modeling method, including the computational domain, computational mesh, input parameters, and simulation methodology.

3.2.1   CFD Modelling of Fluid Region:
The CFD simulations were carried out using ANSYS CFX version 2020 R2. Since the WT rotor is symmetrical about its center of rotation, hence, to reduce simulation time, a single blade replaced the three blades in a 120° domain segment with periodic faces. The schematic of the computational domain along with the boundary conditions is illustrated in Figure 3. The blade's position is five blade lengths from the domain inlet and ten blade lengths from the outlet, while the top wall is six blade lengths from the blade's tip. The blockage ratio of the computational model (the ratio of the

frontal area of the blade to the total domain inlet area) is approximately 0.005 (0.5%), which is sufficiently low to prevent any artificial acceleration. The blade is considered as a stationary non-slip wall, and a rotation frame is created around the blade (as shown in Figure 3) to account for the rotor's rotational speed. This approach avoids the need for a moving mesh and allows for steady-state simulation, reducing computational time.

The general flow regime for the current WT is between 3m/s and 25 m/s, with a preferred operational velocity around 11 m/s, which is the close to the rated wind speed of 10.59m/s [30]. For all cases, a fixed rotational velocity of 5 rpm is applied during the simulations. Figure. 4 presents the unstructured mesh used in the CFD modelling at different critical locations. Figure 4(B) shows the mesh distribution around the blade face while the inflation layers applied to the blade surfaces to appropriately resolve the boundary layer flow as illustrated in Figure 4 (c). Fifteen prismatic inflation layers are used, with an expansion rate of 1.2. The first layer's size is calculated and used so that the y+ value is less than one for the blade surface, as represented in Figure. 5.
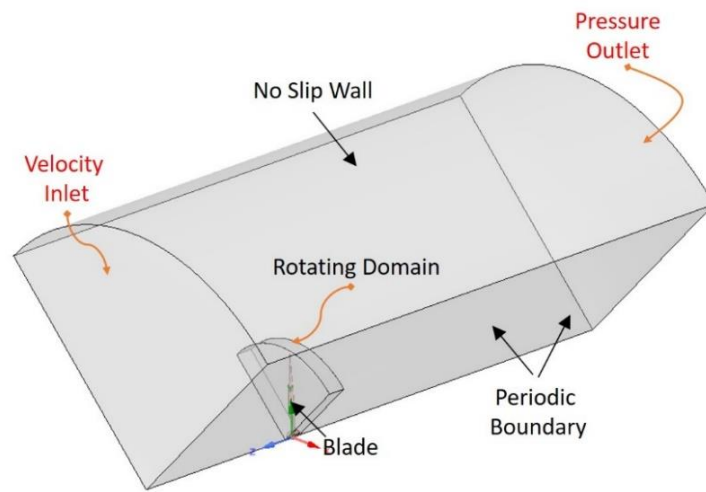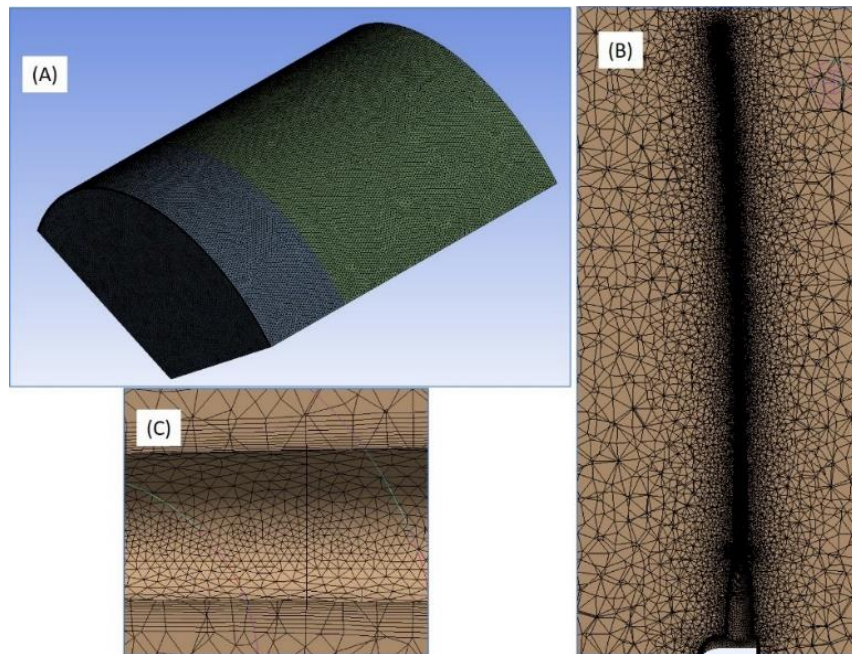

Figure 3: CFD domain and boundary conditions

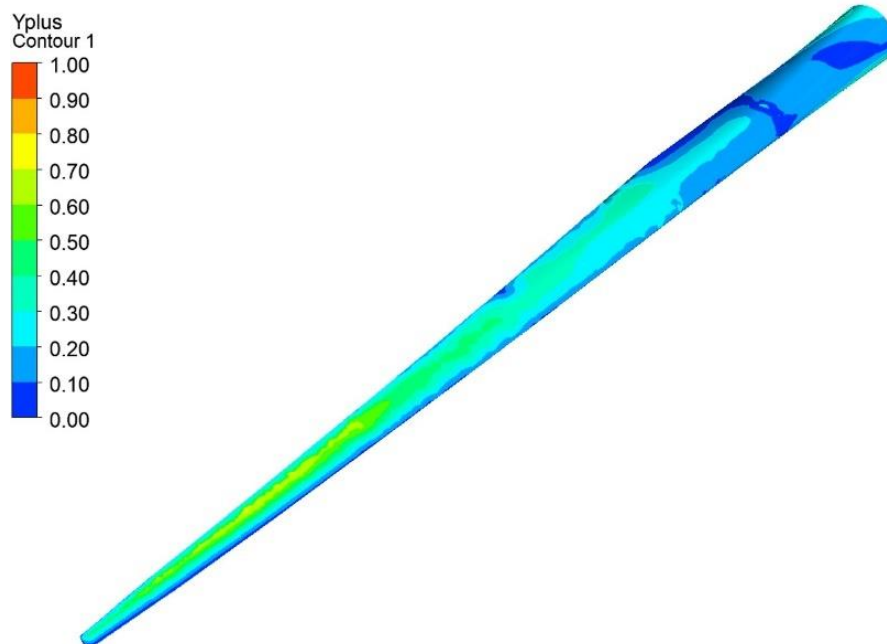**Figure 4: CFD mesh distribution over the simulation domain**

Figure 5: y⁺ distribution on the blade.

To determine the appropriate size of the mesh, a mesh sensitivity analysis was carried out for the wind speed of 8 m/s, blade rotation of 5.7 rpm, and 0 º pitch. For the sensitivity analysis the growth rate (1.15) and max size (6.5m) was fixed, and only the minimum face size was reduced from 1m to 0.001m. The tip velocity of the blade was used as a parameter to check the mesh sensitivity as shown in Table 2. As highlighted in the table, the total element count increased with the increase of mesh density, allowing for a more detailed and accurate flow field representation. The analysis demonstrated that reducing the minimum face size led to changes in tip speed, with diminishing percentage variations, suggesting that a minimum face size of around 0.001 meters could adequately capture flow details while maintaining computational efficiency. This sensitivity analysis guides the present study in selecting an appropriate mesh size for accurate and efficient wind turbine performance modeling.

Table 2: Mesh sensitivity analysis for CFD study

Minimum Face Size (m)	Total Elements (Millions)	Tip Speed (m/s)	Percentage Change (%)
1	1.8	49.006	-
0.5	2.5	56.89	16.08
0.1	3.5	61.05	7.31
0.05	4.5	68.29	11.85
0.0025	5.8	69.85	2.28
0.001	6.2	70.23	0.22

A shear-stress transport (SST) turbulence model is used for this study, which has been used extensively in modelling flow over wind turbine. SST is a robust two-equation model, which has the benefit of swapping from a k-ε turbulence model (well matched for far field) to a k-ω turbulence model (appropriate for boundary layer) [6]. The frozen rotor option of CFX was used, which is a steady-state method and uses the rotating reference frame to save the computational

resources by converting transient turbo-machinery flow into a steady state. The frozen rotor option passes the true flow downstream and vice-versa to capture the downstream wake affect generated by the rotating blade. Despite the low flow speed, there is a high level of turbulence, and abrupt pressure changes occur over short distances. Therefore, the compressible flow option will be utilized for the present study. Moreover, to evaluate the convergence of the CFD analysis in this study, two criteria are employed: residual values and pressure distribution values. The residual serves as a widely used criterion for determining convergence, and a convergence limit of 10-4 was established. Additionally, as the pressure on the blade plays a crucial role in estimating stresses for FEA simulations, the CFD simulations were continuously executed until the average pressure on the blade surface reached a relatively constant value. Once the pressure profile was generated along the blade length, the next step in the FSI modeling was to transfer it to the FEA model to generate the stress and deflection profile of the blade the FEA model to generate the blade's stress and deflection profile. The details of the FEA modelling such as internal blade geometry, blade material properties, composite layups, mesh and boundary conditions are described in the next subsection.

3.2.2 FEA Modeling

This study used ANSYS Static Structural version 2020 R2 to conduct Finite Element Analysis (FEA) simulations. The geometry of the IEA Wind 15-MW Wind Turbine (WT) blade was constructed based on aerodynamic shape information, including airfoil type and location, web location along the span, web thickness, skin thickness, twist, and spar cap thickness, as provided by Gaertner et al. [30]. Table 3 presents a summary of the location and geometric properties of different components. The blade's internal and external geometry was created, comprising skin, two webs, and two spar caps, as depicted in Figure 6(A). Figure 6(B) illustrates the leading edge (LE) web and trailing edge (TE) web, while Figure 6(C) displays the pressure side (PS) and suction side (SS) spar caps. While the original blade and its internal supporting structures consist of multiple components, this study focused on three major components: blade skin, blade webs, and spar caps, as shown in Figure 6.

Table 3: Location wise thickness of different components of the blade.

Airfoil Section	% Span	Web Thickness (m)	Spar Cap Thickness (m)	Skin Thickness (m)
SNL-FFA-W3-500	15	0.040	0.053	0.056
FFA-W3-360	24.51	0.036	0.0838	0.0485
FFA-W3-330blend	32.88	0.032	0.096	0.042
FFA-W3-301	43.91	0.027	0.0957	0.033
FFA-W3-270blend	53.76	0.023	0.0875	0.0256
FFA-W3-241	63.82	0.018	0.0776	0.017
FFA-W3-211	80.11	0.012	0.0434	0.007

Table 4 presents the material properties assigned to each component in this study, along with the original composite material property obtained from the data sheet provided by Gaertner et al. [30]. The leading edge and trailing edge webs, as do the spar caps, have the same thickness. While composite layers are utilized to form each component, a single material is assigned to each component for simplicity in this study. Specifically, glass traix is used for the skin, medium density foam is used for the webs, and Carbon UD for the spar caps. The material properties listed in Table 4 are employed in the FEA simulations, and their respective dimensions are derived from the data presented in [30].

The blade structure is meshed using a hybrid meshing technique, combining tetrahedral and hexahedral elements. The mesh distribution on the blade skin, webs, and spar caps is illustrated in Figure 7. Figure 7(B) specifically demonstrates the mesh distribution on the spar caps and webs. Following a mesh sensitivity analysis, specific mesh parameters were selected, including a minimum face size of 0.001m, a growth rate of 1.15, and a maximum size of 0.1 m, resulting in a total of 750,000 elements generated for the model. The WT blade is subjected to various types of loads, and for this study, three specific loads are considered. Firstly, the aerodynamic load, i.e., pressure loads, is imported from the CFD simulations. Secondly, gravity loads are accounted for, considering the blade's weight. Lastly, centrifugal loads resulting from the rotation of the blades are also incorporated. Both gravity and centrifugal loads are applied as boundary conditions in the FEA simulator. To simulate the fixed support at the blade's interface with the hub, a fixed support boundary condition is applied at the beginning of the blade. This ensures the appropriate modeling of the blade's connection with the hub, providing accurate and realistic results for the subsequent analyses.
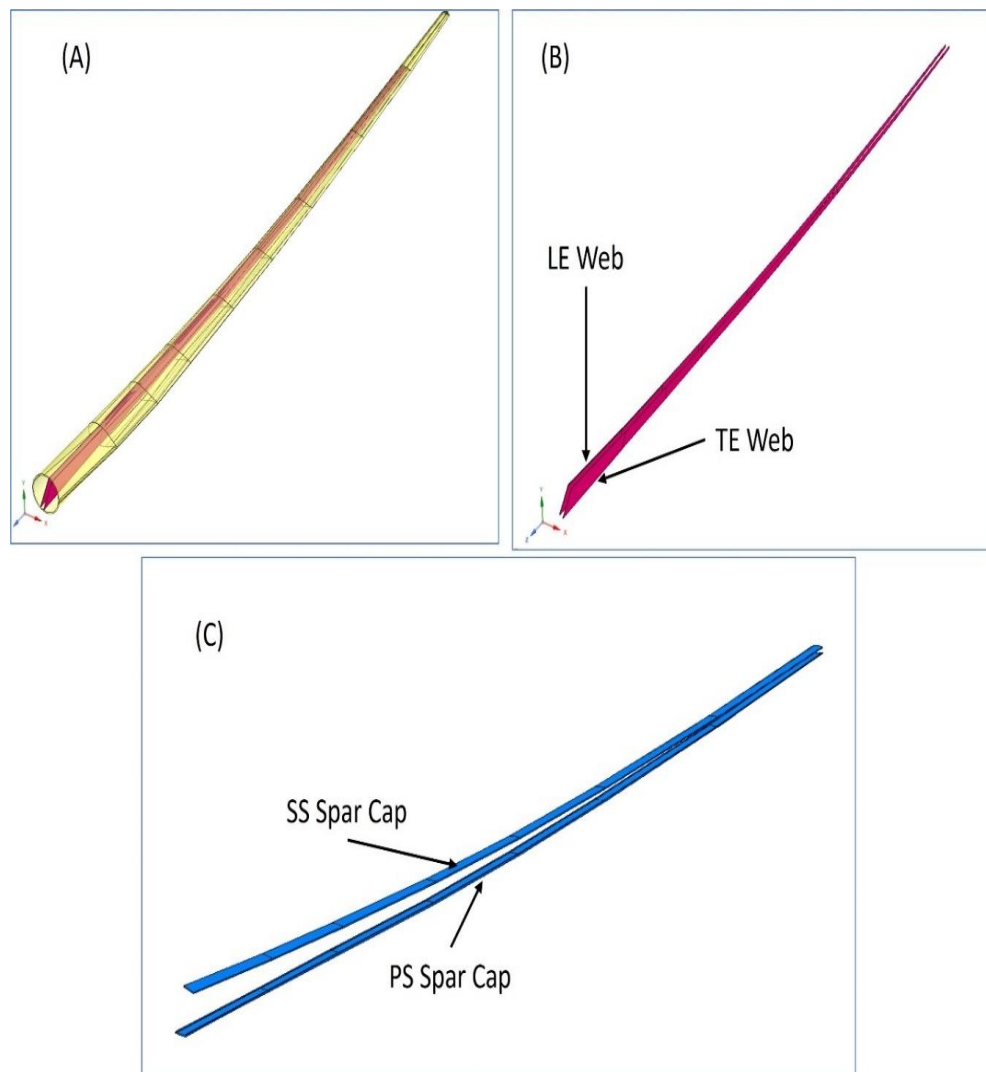

Figure 6: CAD model of components of wind turbine blade used for FEA modeling

Table 4: Material properties for blade components

Material Properties	Medium_Density_Foam	Carbon UD	Glass Traix
Density [kg/m^3]	130	1220	1940
Young Modulus E_1 [MPa]	129.2	114500	44600
Young Modulus E_2 [MPa]	129.2	8390	17000
Young Modulus E_3 [MPa]	129.2	8390	16700
Shear Modulus G_1 [MPa]	48.946	5990	3270
Shear Modulus G_2 [MPa]	48.946	5990	3480
Shear Modulus G_3 [MPa]	48.946	5990	3500
Poisson ratio nu_1	0.32	0.27	0.262
Poisson ratio nu_2	0.32	0.27	0.35
Poisson ratio nu_3	0.32	0.27	0.264
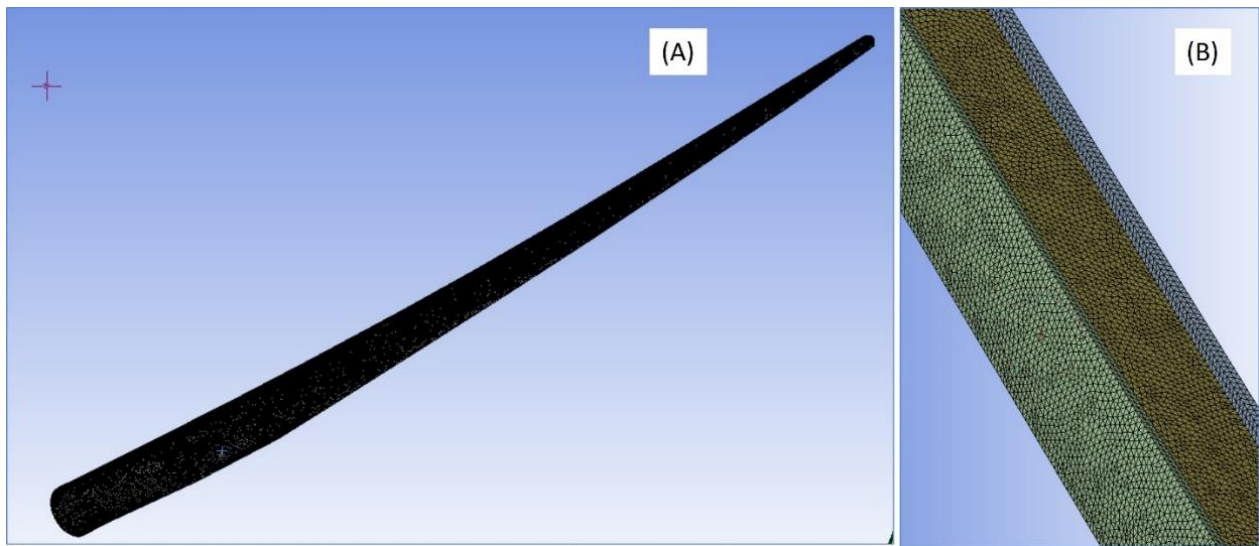
Figure 7: FEA mesh distribution for the blade components

Overall, the modeling approach and load considerations in this study have been meticulously selected and implemented to accurately capture the complex structural behavior of the wind turbine blade. The combination of CFD and FEA simulations allows for a comprehensive analysis of the blade's response to the different types of loads it experiences during operation. The results of the FSI modeling are discussed in the next sub-section.

3.2.3 FSI Modeling Results

From the results perspective, we focus on two crucial parameters, namely von Mises stress and deflection, for analyzing the wind turbine blade. To enhance clarity and avoid overwhelming the readers with excessive data, we present the results at nine carefully selected locations (L1 to L9) along the blade length, as depicted in Figure 2. These locations also indicate the change in the airfoil geometry and hence the location of supports. This approach allows for a more targeted and informative presentation of the findings, facilitating a comprehensive understanding of the blade's structural performance. The simulation was conducted for eight distinct wind speeds, specifically

3 m/s, 9 m/s, 11 m/s, 12.5 m/s, 15 m/s, 17.5 m/s, 21 m/s, and 25 m/s. The outcomes of the simulation are graphically depicted in Figure 8.
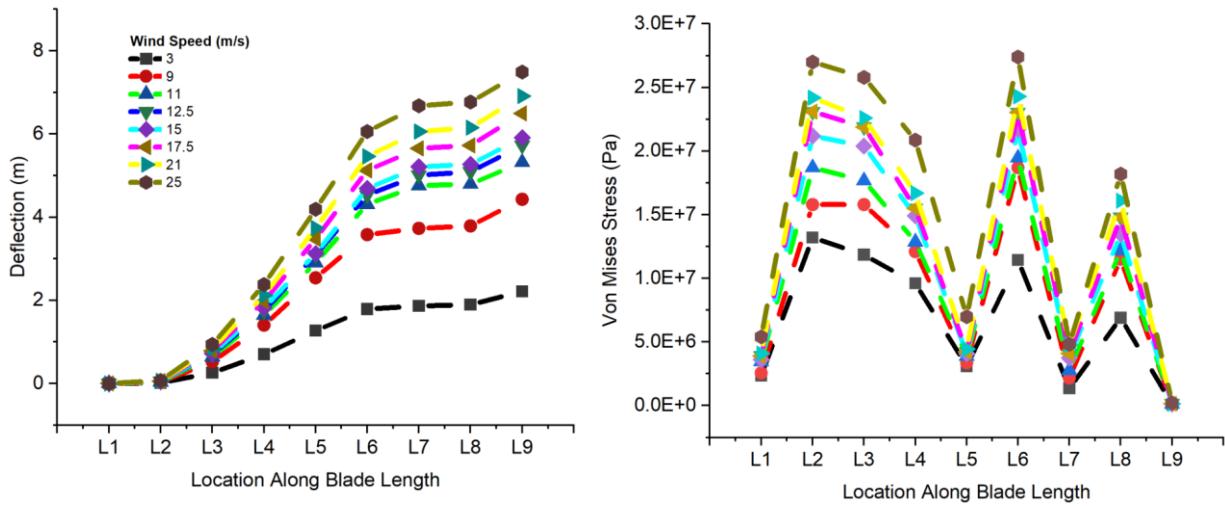

Figure 8: FSI Simulation results for Deflection (Left) and Von Mises stress (Right) along the blade length

Two noteworthy observations can be deduced from the FSI simulation outcomes depicted in Figure 8. Firstly, there is a noticeable increase in deflection at a specific location with the augmentation of the free stream velocity. This phenomenon can be attributed to the concurrent increase in pressure force, directly influenced by the velocity escalation. Similarly, an analogous observation can be drawn for von Mises stress, wherein the stress at a given location rises in tandem with the augmentation of the free stream velocity. Secondly, a distinct trend emerges where in deflection progressively augments as we traverse away from the hub, culminating in the maximum deflection being encountered at the blade tip. This behavior is akin to that of a cantilever structure. Notably, this trend is not mirrored in the von Mises stresses, a characteristic arising from the blade's inherent twist.

The outcomes of the FSI simulations play a pivotal role in the subsequent section, where they are employed to construct a SM for the FSI simulator. This strategic utilization of simulation results aids in significantly reducing computational time, a critical consideration for efficient analysis.

3.3 Surrogate Model Development

3.3.1 Data Analysis

The complete dataset comprises seventy-two rows, resulting from the multiplication of nine distinct locations by eight varying wind speeds. Each row is characterized by four columns: Location on Blade, Wind Speed, Von Mises stress, and Deflection. Initial data analysis of the FSI outcomes entails comprehensively exploring parameter distributions and interrelationships. These graphical tools provide insights into the intricate connections among the diverse parameters, offering a foundational understanding of the dataset's underlying structure and dynamics. First, we generate a pair-plot matrix and subsequently constructing a correlation matrix. A pair plot is essential in data analysis due to its ability to reveal intricate patterns and relationships within a multidimensional dataset. As a powerful graphical tool, a pair plot enables the simultaneous visualization of multiple variables in a matrix-like arrangement as depicted in Figure 9. This holistic approach facilitates the identification of potential associations, trends, and correlations

between different variables. The results from the pair-plot matrix indicates how different parameters are related to each other. The most interesting relationship is exhibited in the bottom left scatter plot (indicating relationship between deflection, wind speed and location). For higher wind speeds the deflection is larger and the deflection increases as we move from blade root (L1) to blade tip (L9) as expected. The histogram for wind speed (shown in top left) has a uniform distribution indicating equal probability of occurrence of the eight wind speeds. The other histograms along the diagonal doesn't follow any pattern.
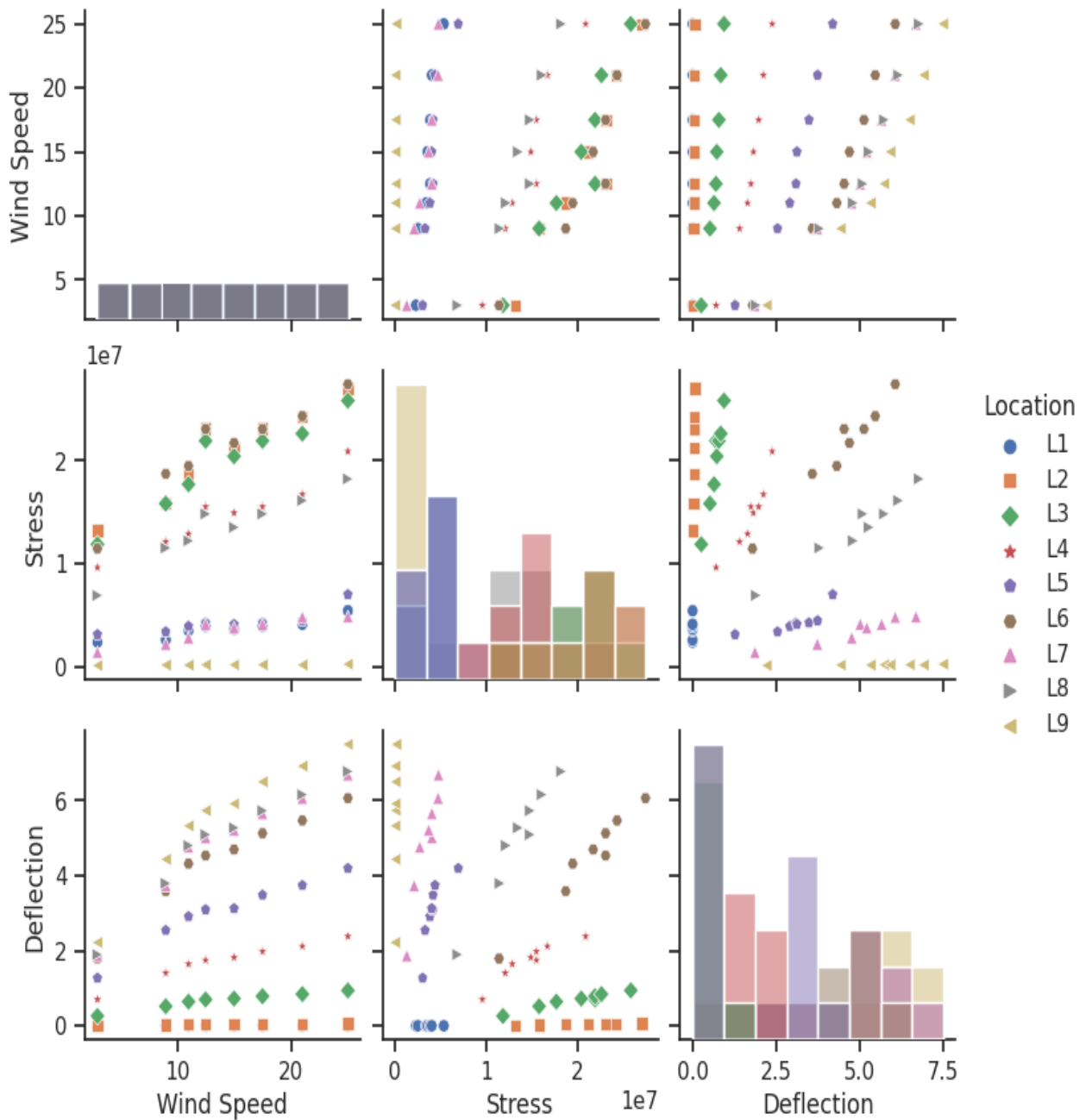

Figure 9: Pair plot matrix of different variables

Subsequently, we construct the Pearson correlation matrix to quantify the linear associations between variable pairs, revealing vital insights into their strength and directional relationships. Illustrated in Figure 10, the Pearson correlation matrix underscores the positive correlation between deflection, blade location, and wind speed. This suggests that deflection increases with greater wind speeds and at positions farther from the blade's root. Conversely, deflection
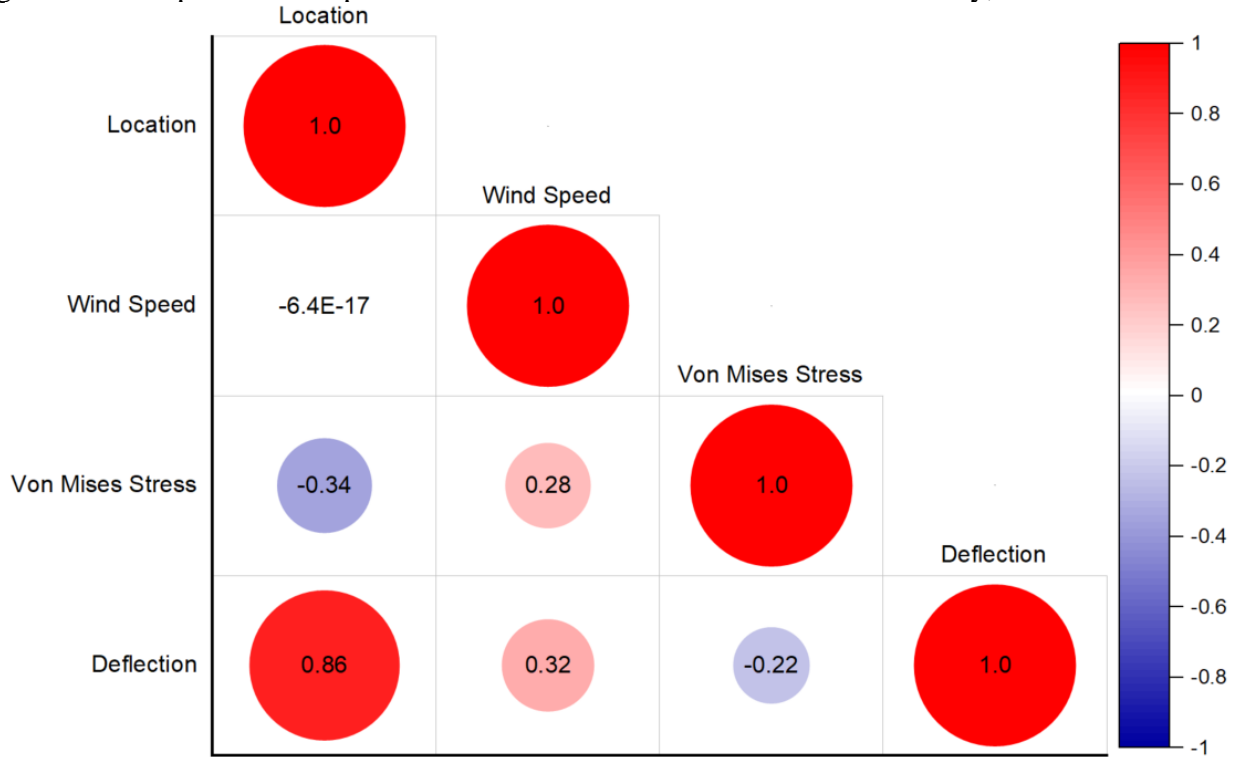

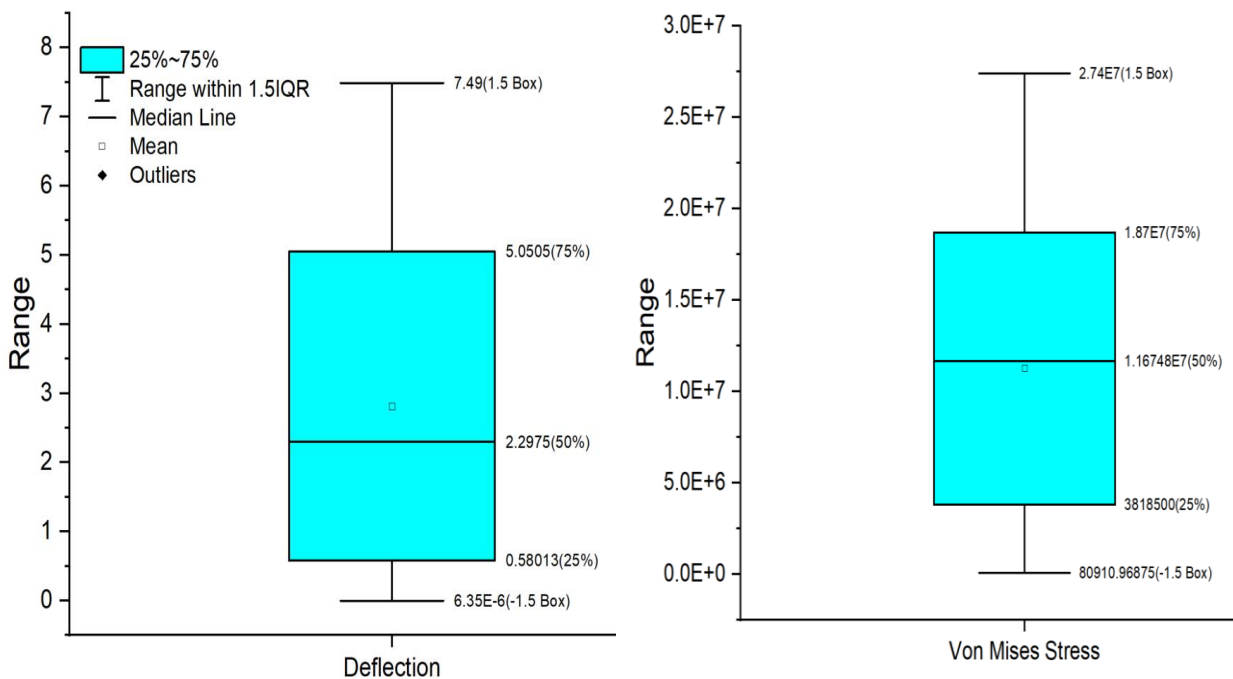**Figure 10: Pearson Correlation Matrix of different variables**

Figure 11: Box Plot indicating 5-point summary for Deflection (Left) and von Mises stress (Right)

demonstrates a weak negative correlation with von Mises stress. In addition to these analyses, addressing potential outliers within the dataset is imperative. Hence, we employ box plots for deflection and von Mises stress, as presented in Figure 11, depicting the five-point summary—encompassing minimum, maximum, and quartiles. This examination underscores the absence of outliers in the dataset, a crucial prerequisite before employing it for the training and testing of machine learning models.

3.3.2 *Kriging Model Development and Results*

Following the completion of data analysis, the simulation results are partitioned into distinct training and testing datasets. Specifically, the simulation outcomes corresponding to wind speeds of 12.5 m/s and 17.5 m/s, comprising 18 data points, are earmarked as test data. The chosen wind speeds represent distinct, operationally relevant scenarios, ensuring a comprehensive and robust evaluation of the Kriging model across varied conditions. These speeds were selected based on their ability to provide a diverse and representative dataset, ensuring the model is validated under both moderate and high operational wind conditions, which are crucial for assessing structural reliability and safety. The remaining dataset, encompassing 54 data points, is utilized for model training via k-fold cross-validation. This strategic data partitioning approach yields advantages by iteratively alternating between training and testing subsets, enhancing model performance metrics' reliability and generalization. Ensuring the appropriateness of the chosen k value in relation to the dataset size is crucial; for our dataset, a value of 10 was selected to maintain representation adequacy, particularly beneficial for smaller datasets. Subsequently, leveraging blade location, wind speed, and von Mises stress as input parameters, along with blade deflection as the output measure, we initially train the Kriging model with default hyperparameters. However, Kriging models encompass distinct hyperparameters (as detailed in Table 5) necessitating a meticulous selection process by analysts to optimize predictive accuracy. Bayesian Optimization, chosen for its heightened efficacy and expedited convergence relative to Grid Search and Random Search, comprehensively explores the hyperparameter space to determine the optimal Kriging model. Over a span of 30 iterations, the 25th iteration yields the minimal Mean Squared Error (MSE), as indicated by red-highlighted values in Table 5.

A performance comparison between the non-optimized and optimized Kriging models is presented in Figure 12 and Table 6. The discernible outcomes affirm the superior performance of the latter model, attributed to the incorporation of optimized hyperparameters albeit with a prolonged training phase. Subsequently, the optimized model is applied to predict deflection for two distinct test datasets. Model performance, compared with FSI simulation results, is depicted in Figure 13. The discernment from Figure 13 and evaluation metrics underscores the anticipated superiority of the model's performance on the training set. Furthermore, the model exhibits superior performance on test_data_2 (i.e., wind speed of 17.5 m/s) in comparison to test_data_1 (wind speed of 12.5 m/s), a finding corroborated by the metrics in Table 5 and Figure 13. Notably, the higher R^2 values for both test datasets substantiate the Kriging model's viability as a surrogate for computational-intensive FSI simulations. This surrogate model is harnessed in next step to predict blade tip deflection across the entire wind speed spectrum. Additionally, we employ cubic spline interpolation to construct an envelope for predicting blade deflection. This envelope spans wind speeds from 0 m/s to 30 m/s, with intervals of 0.5 m/s (we have to discretizing the input space in order to save time), and covers the entire length of the blade, as depicted in Figure 14. It is important to note that predicting blade deflection for a single wind speed through FSI simulations requires approximately 10 minutes, contingent upon mesh refinements. Consequently, for the

entire range of wind speeds spanning from 0 to 30 m/s in intervals of 0.5 m/s, the cumulative time required is approximately 7 hours. However, using the optimized Kriging model, the blade deflection for same wind interval is obtained in about 1minute. Thus, showcasing that developed Kriging model is about 400 times faster than the FSI simulations.

Table 5: Hyperparameters search space for Kriging Model

| Hyper Parameter Name	Possible Value
Basis Function	Zero, Constant, Linear
Kernel Function	Nonisotropic Squared Exponential, Isotropic Squared Exponential, Nonisotropic Rational Quadratic, Isotropic Rational Quadratic, Nonisotropic Matern 5/2, Isotropic Matern 5/2, Nonisotropic Matern 3/2, Isotropic Matern 3/2, Nonisotropic Exponential, Isotropic Exponential
Kernel Scale	real values in the range [0.001,1]*max(max(X) – min(X)) where X is the predictor data. Optimized Value = 3.868
Sigma	real values in the range [0.0001, max (0.001,10*std(Y))], where Y is the response variable. Optimized Value = 1.665
Standardize	True, False
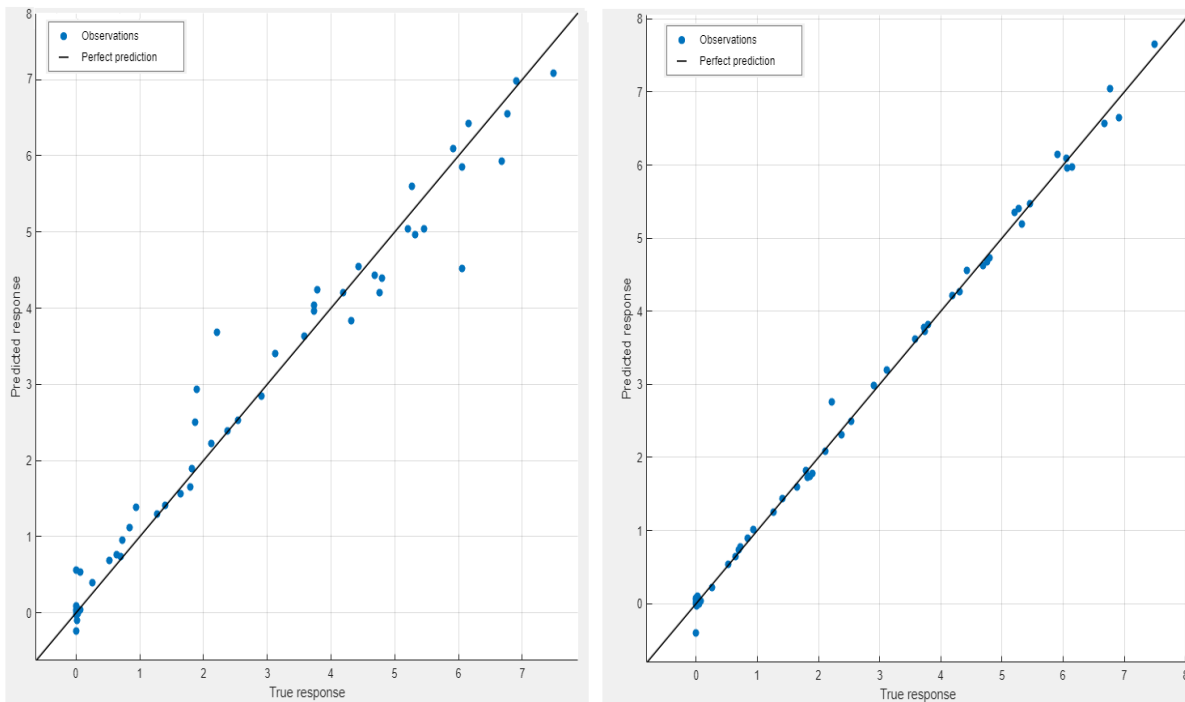
Figure 12: Performance of the non-optimized (Left) vs optimized Kriging (Right) model

Table 6: Comparison of Kriging Model

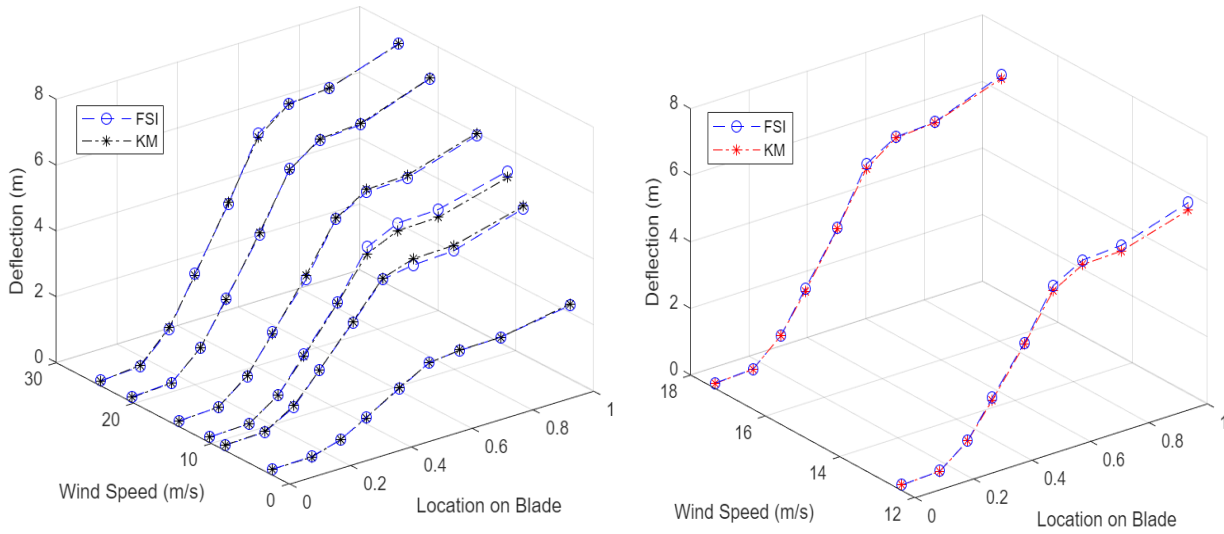| Evaluation Metrics	Non-Optimized Kriging Model	Optimized Kriging Model (Validation)	Optimized Kriging Model (Test)
RMSE	0.422	0.203	0.124 (test_set_1) 0.066 (test_set_2)
R^2	0.94	0.999	0.989 (test_set_1) 0.997 (test_set_2)
Training Time	1.369	26.67	N. A

Figure 13: FSI vs. KM prediction of deflection on training (left) and testing (right) dataset

3.4 Reliability Analysis Results

The initial step in conducting reliability analysis involves the selection of an appropriate distribution for the capacity and demand variables. In the context of WT rotor blade loads, which are directly proportional to wind speed, it is essential to opt for an accurate wind speed distribution to effectively represent these loads. Within the literature concerning wind resource potential assessments, various probability distributions, including Rayleigh, Gamma, Nakagami, Generalized Extreme Value, and Weibull, have been considered [39]. Given that the Weibull distribution is widely utilized for characterizing wind speed probability distributions and extreme load distributions due to its capacity to capture attributes like skewness and extended tails, this study follows suit by employing the Weibull distribution to model wind speed [31]. In our case study, we have selected the Havoygavlen wind park site in Northern Norway, where the Weibull distribution is defined by parameters 1.96 (shape) and 9.4 (scale) [39].

Subsequently, a million wind speed samples are generated from the Weibull distribution and input into the optimized Kriging model (obtained in previous step) to derive blade tip deflection outcomes (refer to Fig. 1). Following this, a kernel density estimate of blade tip deflection is acquired, and a normal distribution is fitted to the projected values. As illustrated in Fig. 15, the fitted normal distribution, characterized by a mean of 4.193 [4.190 - 4.195] and a standard

deviation of 1.302 [1.300 – 1.304], demonstrates a reasonable fit. The values enclosed within the square brackets denote the 95% confidence interval (CI) for both parameters. This fitted normal distribution is subsequently employed as the demand distribution (referred to as variable S in Equation 8) for the purpose of reliability analysis.
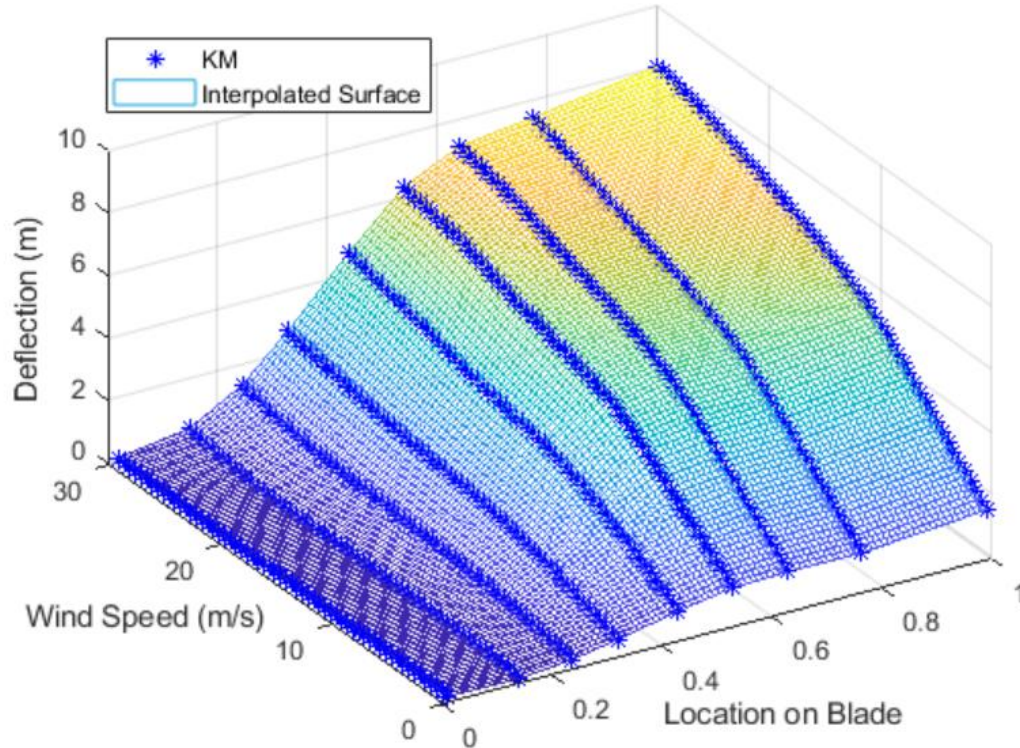

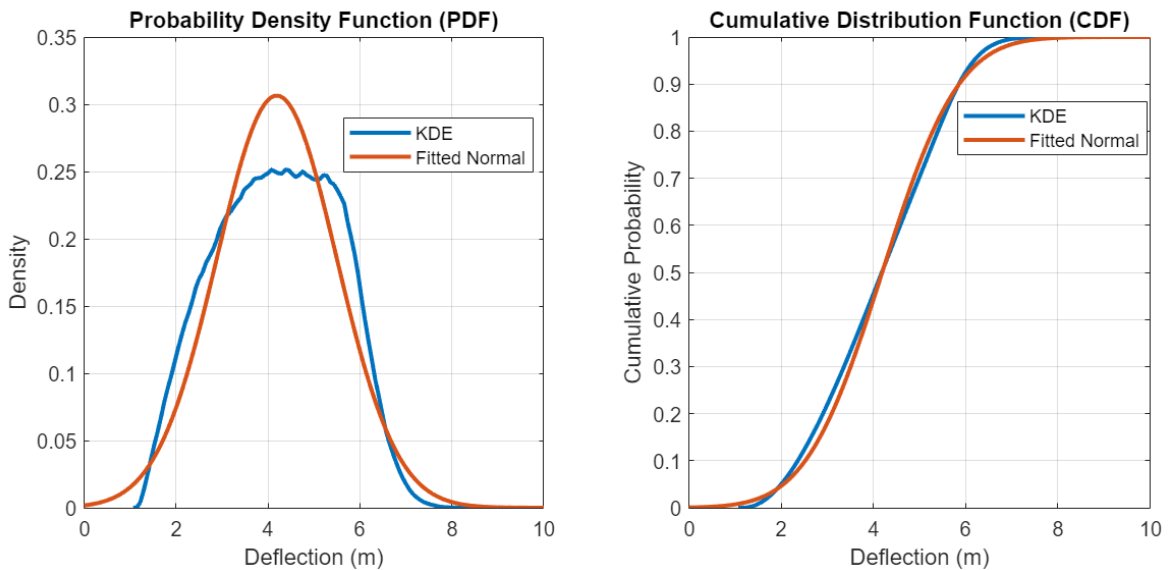**Figure 14: Interpolated surface that can be used for predicting blade deflection**

Figure 15: PDF (Left) and CDF (Right) of fitted normal distribution and associated KDE

In the subsequent phase, the selection of a representative probability distribution for the capacity variable (R) becomes pivotal. The maximum out-of-plane blade tip deflection of a particular wind turbine is subject to fluctuations influenced by diverse factors, encompassing turbine design, environmental conditions, and operational parameters. For the sake of simplicity, we adopt a normal distribution with a mean of 12.5 and a standard deviation of 3 (the latter indicating a higher degree of uncertainty due to limited data availability). This distribution is deemed suitable for the resistance variable, denoting allowable blade tip flap-wise deflection. However, it is prudent to consult wind energy experts, undertake statistical analysis of available data, and account for the blade's resistance within the framework of physical behavior and engineering principles.

After that, we employ MCS, wherein one million samples are generated from the R and S distributions (illustrated in Figure 16). Subsequently, utilizing the limit state function as defined in Eq. 8, the P_f is computed. Figure 17 displays the convergence plot of P_f alongside the corresponding values. However, owing to extended computation time, gradual convergence, and suboptimal sampling strategy, we implement Adaptive Kriging Monte Carlo Simulation (AKMCS) for the reliability analysis. AKMCS is designed to enhance the efficiency of the MCS process by dynamically refining the Kriging surrogate model as additional simulation runs are executed. This optimization revolves around the judicious selection of new sample points, leveraging insights from the surrogate model concerning uncertainty. The focus of this sampling strategy centers on regions characterized by elevated uncertainty or requiring precise estimation, notably in proximity to the limit state function (depicted in Figure 17). Consequently, it leads to an enhanced sample efficiency compared to conventional MCS. Moreover, this sampling approach leads to accelerated convergence (requiring only 21 samples for AKMCS, as opposed to 1 million samples for MCS as shown in Figure 18) while maintaining a negligible reduction in the precision of the estimated probability of failure (Pf) and reliability index (β), as indicated by the coefficients of variation (CoV) values presented in Table 7. Subsequently, the estimated reliability index (β) derived through AKMCS is juxtaposed with the predefined threshold β, triggering an inspection when the threshold is exceeded.
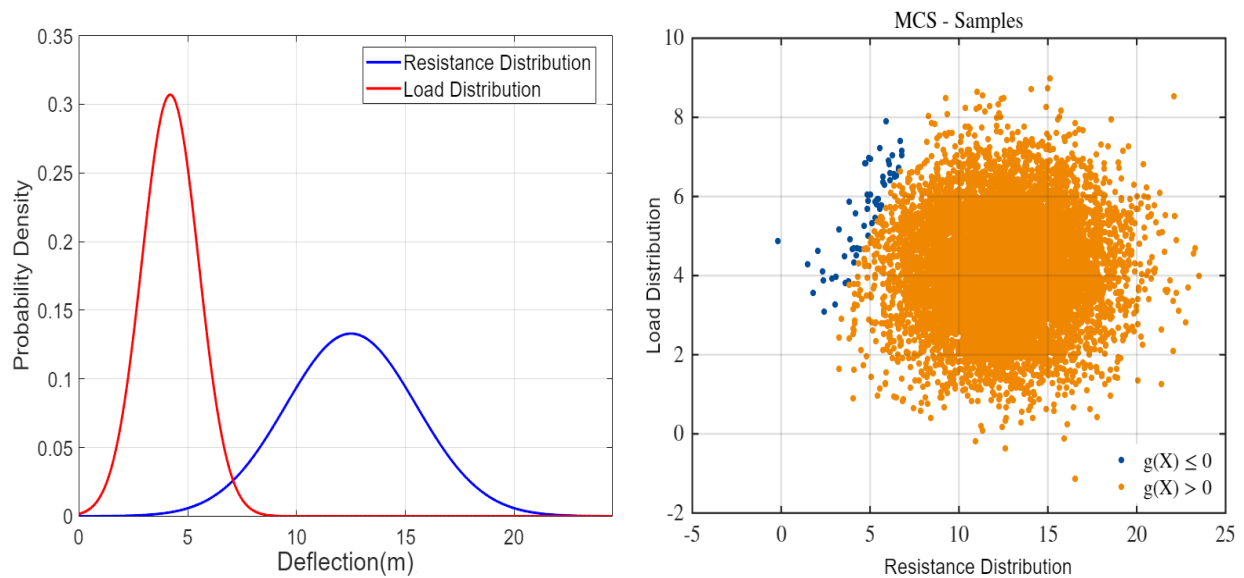

Figure 16: Load and Resistance Distributions (Left) along with generated samples via MCS (Right)
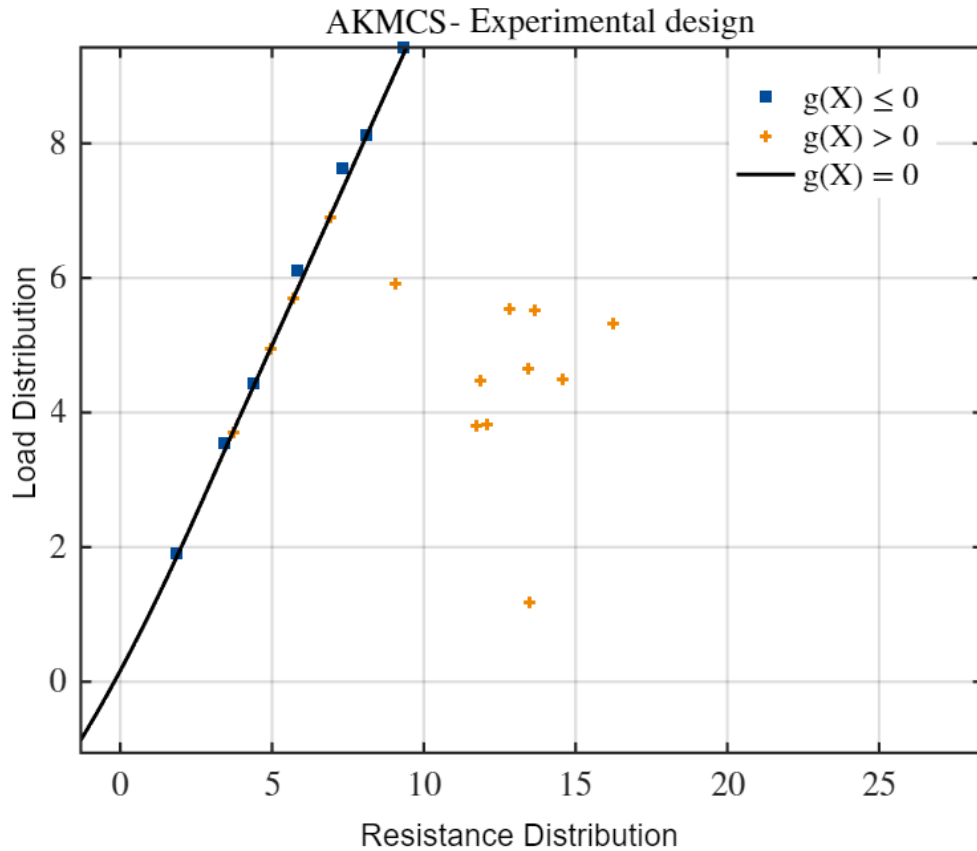
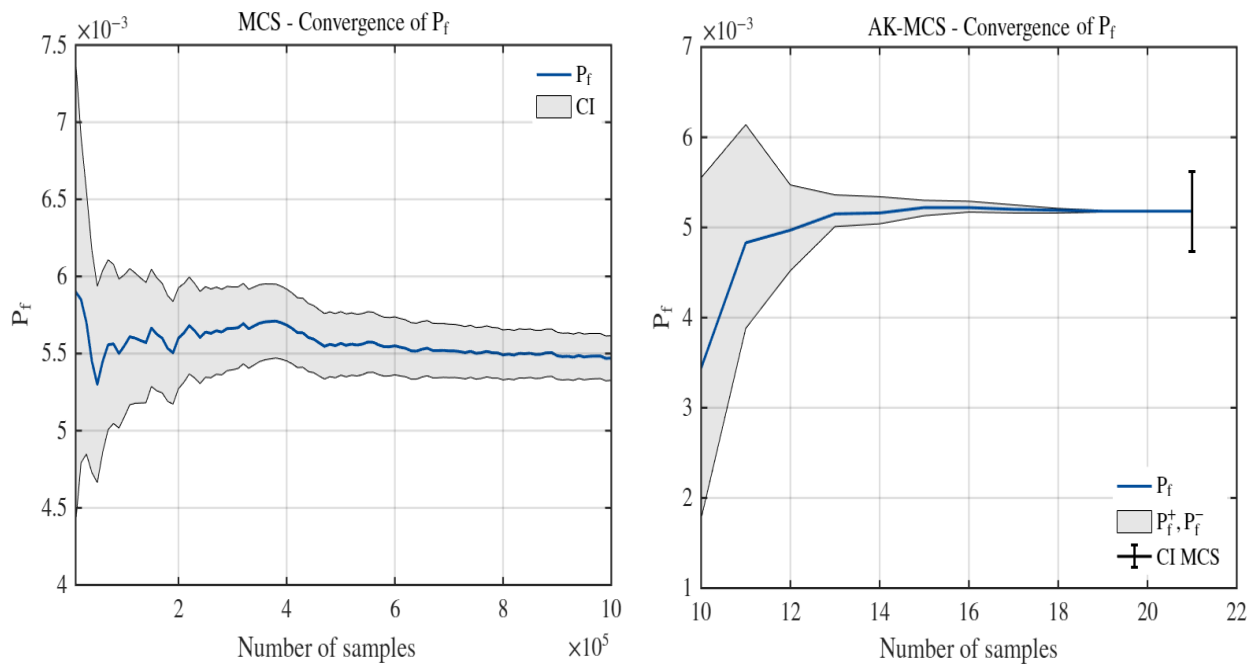**Figure 17: Samples generated using AKMCS strategy**

Figure 18: Comparing failure probability convergence for MCS (Left) and AKMCS (Right)

Table 7: Comparison of MCS and AKMCS

Parameter	MCS	AKMCS
Probability of failure (P_f)	5.47e-03	5.18e-03
Reliability Factor (β)	2.544	2.5636
Coefficient of Variation (CoV)	0.0135	0.0438
Number of Samples	1 million	21
P_f _CI	[5.326e-03, 5.615e-03]	[4.735e-03, 5.624e-03]
β_CI	[2.535, 2.553]	[2.534, 2.594]

4. Future Direction: Pioneering the Digital Twin Concept

The promising outcomes of this research pave the way for an exciting avenue of future exploration - integrating the proposed methodology into the creation of WT digital twins. The concept of digital twins involves the development of virtual replicas of physical assets, allowing real-time monitoring, analysis, and predictive maintenance. By leveraging the capabilities of the combined FSI simulations and the efficient Kriging model, the potential for building accurate and dynamic digital twins for wind turbines emerges.

The envisaged digital twin would embody the intricate interplay between aerodynamics, structural dynamics, and reliability parameters, providing an insightful glimpse into the operational behavior of wind turbines. Real-time monitoring of deflection, stress distribution, and reliability metrics could be seamlessly integrated into the digital twin framework, facilitating continuous health assessment and performance optimization. The Kriging model's rapid prediction capabilities align well with the dynamic nature of digital twins, ensuring prompt updates and responsiveness to changing operating conditions.

Moreover, successfully adapting this methodology into the digital twin realm could transcend the domain of WT reliability analysis. The holistic approach, encompassing data-driven SM and advanced statistical techniques, could potentially find applications in diverse fields such as aerospace, civil engineering, and automotive industries. The utilization of digital twins for predictive maintenance, operational optimization, and risk mitigation holds substantial promise, and this research opens a pathway towards its realization. Amidst the ongoing growth and innovation in the wind energy sector, exploring the integration of the proposed methodology into digital twin frameworks is a promising avenue. Such an endeavor holds the potential to substantially bolster operational efficiency, reliability, and sustainability, making it a compelling subject warranting rigorous research investigation.

5. Conclusions

In this paper, we proposed a methodology that couples FSI simulation, Kriging algorithm, and AKMCS to perform reliability analysis of the 15MW IEA reference HAWT rotor blades. Central to this approach is optimizing a Kriging model, which is trained and tested using the dataset derived from the FSI simulations. In the context of FSI simulations, the load transfer method is

employed, with independent resolution of the fluid and structure domains utilizing ANSYS CFX and ANSYS Structural software. The pressure profiles derived from Computational Fluid Dynamics (CFD) simulations are seamlessly transferred to the Finite Element Analysis (FEA) model, subsequently providing Von-Mises Stress and displacement profiles along the entire blade length. Employing diverse data analysis techniques including pair plot matrix, Pearson correlation matrix, and box plots, we comprehensively analyze the FSI dataset. Pearson correlation matrix underscores the positive correlation between deflection and blade location and wind speed while deflection demonstrated a weak negative correlation with Von-Mises Stress. The box plots underscored the absence of outliers in the dataset, which is crucial prerequisite before employing dataset for the training and testing of Kriging models.

The dataset is further stratified into training and test sets, with the K-fold cross-validation approach adopted during the training of the Kriging model. This model, initially trained using default hyperparameters, is subsequently fine-tuned using Bayesian Optimization to enhance its performance. Significantly, the optimized Kriging model functions as a surrogate for computationally intensive FSI simulations, enabling blade deflection prediction at a remarkable speed, surpassing FSI simulations by a factor of 400 while maintaining exceptional accuracy. Leveraging this optimized surrogate model, we project flap-wise blade tip deflection across a spectrum of one million wind speeds generated from the Weibull distribution. Subsequently, a limit state function is formulated. Thereby, applying statistical modeling techniques, notably Monte Carlo Simulation (MCS) and AKMCS, we ascertain the reliability of the rotor blades. Remarkably, AKMCS demonstrates rapid convergence, demanding only 21 samples, in stark contrast to the resource-intensive requirement of 1 million samples for conventional MCS. This remarkable acceleration in convergence is achieved without compromising the precision of the estimated probability of failure (Pf) and reliability index (β).

The significant implications of this research extend beyond its immediate application. The promising results of our study lay the foundation for integrating this methodology into the creation of digital twins for WTs. This holistic approach, enriched with data-driven surrogate modeling and advanced statistical techniques, holds the promise of applications across diverse sectors like aerospace, civil engineering, and automotive industries.

6. References

1.   Horowitz, C.A., Paris agreement. International Legal Materials, 2016. 55(4): p. 740-755.
2.   Chen K, Song MX, Zhang X, Wang SF. Wind turbine layout optimization with multiple hub height wind turbines using greedy algorithm. Renew Energy 2016; 96:676–86.
3.   https://www.iea.org/reports/wind-electricity.
4.   Larwood, S. M. (2014). Design Studies of Swept Wind Turbine Blades. Renewable Energy, 71, 563–571. https://doi.org/10.1016/J.RENENE.2014.05.050
5.   Kim, B.-S. (2011). Aerodynamic design and performance analysis of multi-MW class wind turbine blade. Journal of Mechanical Science and Technology, 25(8), 1995–2002.
6.   Wang, L., R. Quant, and A. Kolios, Fluid structure interaction modelling of horizontal-axis wind turbine blades based on CFD and FEA. Journal of Wind Engineering and Industrial Aerodynamics, 2016. 158: p. 11-25.
7.   Grinderslev, C., S. González Horcas, and N.N. Sørensen, Fluid–structure interaction simulations of a wind turbine rotor in complex flows, validated through field experiments. Wind Energy, 2021.

8. Tangler, J. and D. Kocurek. Wind turbine post-stall airfoil performance characteristics guidelines for blade-element momentum methods. in 43rd AIAA Aerospace Sciences Meeting and Exhibit. 2005.

9. Fernandez, G., H. Usabiaga, and D. Vandepitte, An efficient procedure for the calculation of the stress distribution in a wind turbine blade under aerodynamic loads. Journal of Wind Engineering and Industrial Aerodynamics, 2018. 172: p. 42-54.

10. Lanzafame, R. and M. Messina, BEM theory: How to consider the radial flow inside of a 1-D numerical code. Renewable Energy, 2012. 39(1): p. 440-446.

11. Shen, W. Z., Lu, L., & Sørensen, J. N. (2014). Investigating the aerodynamic performance of a horizontal axis wind turbine using blade element momentum theory. Energy, 77, 610-619.

12. Shives, M., & Schreck, S. (2017). Performance analysis of variable pitch wind turbines using blade element momentum theory. Journal of Physics: Conference Series, 854(1), 012004.

13. Barlas, T. K. (2014). A comparison of two methods for simulating the unsteady aerodynamics of wind turbines. Journal of Physics: Conference Series, 555(1), 012017.

14. Gebraad, P. M., Teeuwisse, F. W., & Van Wingerden, J. W. (2016). Optimal rotor control strategies for wind turbines under turbulent wind conditions. Renewable Energy, 96, 471-485.

15. Cheng, P. W., Yang, T., & Li, J. (2020). Aerodynamic design and performance analysis of a small wind turbine using blade element momentum theory. Energy Conversion and Management, 220, 113100.

16. Sayed, M. A., & El-Badawy, A. A. (2011). Unsteady aerodynamic simulation of horizontal axis wind turbine blade. In World wind energy conference, Cairo, Egypt.

17. Madsen, H. A., Riziotis, V., Zahle, F., Hansen, M. O. L., Snel, H., Grasso, F., ... & Rasmussen, F. (2012). Blade element momentum modeling of inflow with shear in comparison with advanced model results. Wind Energy, 15(1), 63-81.

18. Cai, X., et al., Unsteady aerodynamics simulation of a full-scale horizontal axis wind turbine using CFD methodology. Energy Conversion and Management, 2016. 112: p. 146-156.

19. Bazilevs, Y., et al., 3D simulation of wind turbine rotors at full scale. Part II: Fluid–structure interaction modeling with composite blades. International Journal for numerical methods in fluids, 2011. 65(1-3): p. 236-253.

20. Korobenko, A., et al., Structural mechanics modeling and FSI simulation of wind turbines. Mathematical Models and Methods in Applied Sciences, 2013. 23(02): p. 249-272.

21. Lee, K., et al., Fluid-structure interaction analysis of NREL phase VI wind turbine: Aerodynamic force evaluation and structural analysis using FSI analysis. Renewable Energy, 2017. 113: p. 512-531.

22. Patel, Y.R., FSI in Wind Turbines: A Review. Int. J. Recent Contributions Eng. Sci. IT, 2020. 8(3): p. 37-50.

23. Shourangiz-Haghighi, A., et al., State of the art in the optimisation of wind turbine performance using CFD. Archives of Computational Methods in Engineering, 2020. 27(2): p. 413-431.

24. Keprate, A., R.M.C. Ratnayake, and S. Sankararaman, Adaptive Gaussian process regression as an alternative to FEM for prediction of stress intensity factor to assess fatigue degradation in offshore pipeline. International Journal of Pressure Vessels and Piping, 2017, Vol. 153: p. 45-58.

25. Zhou, L., Wen, J., Wang, Z., Deng, P., & Zhang, H. (2023, July). High-fidelity wind turbine wake velocity prediction by surrogate model based on d-POD and LSTM. Energy, 275, 127525.

26.   Wilson, B., S. Wakes, and M. Mayo. Surrogate modeling a computational fluid dynamics-based wind turbine wake simulation using machine learning. in 2017 IEEE Symposium Series on Computational Intelligence (SSCI). 2017. IEEE.

27.   Richmond, M., et al., Stochastic assessment of aerodynamics within offshore wind farms based on machine-learning. Renewable Energy, 2020. 161: p. 650-661.

28.   Bagalkot, N., A. Keprate, and R. Orderløkken, Combining Computational Fluid Dynamics and Gradient Boosting Regressor for Predicting Force Distribution on Horizontal Axis Wind Turbine. Vibration, 2021. 4(1): p. 248-262.

29.   Morató, A., Sriramula, S., & Krishnan, N. (2018, September 26). Kriging models for aero-elastic simulations and reliability analysis of offshore wind turbine support structures. Ships and Offshore Structures, 14(6), 545–558.

30.   Gaertner, E., et al., 2020, Definition of the IEA 15-Megawatt Offshore Reference Wind Turbine. 2020, National Renewable Energy Lab (NREL), Golden, CO (United States), NREL/TP-5000-75698.

31.   Rinne H. The Weibull Distribution: A Handbook. CRC Press; 2008.

32.   Grinderslev, C., Horcas, S. G., & Sørensen, N. N. (2021). Fluid–structure interaction simulations of a wind turbine rotor in complex flows, validated through field experiments. Wind Energy, 24(12), 1426–1442.

33.   Wang, J., Sun, Z., & Cao, R. (2021, December). An efficient and robust Kriging-based method for system reliability analysis. Reliability Engineering & System Safety, 216, 107953.

34.   Hwang, S. G., L'Huillier, B., Keeley, R. E., Jee, M. J., & Shafieloo, A. (2023, February 1). How to use GP: effects of the mean function and hyperparameter selection on Gaussian process regression. Journal of Cosmology and Astroparticle Physics, 2023(02), 014.

35.   Haldar, A., & Mahadevan, S. (1999, November 1). Probability, Reliability, and Statistical Methods in Engineering Design.

36.   Alibrandi, U., Alani, A. M., & Ricciardi, G. (2015, July). A new sampling strategy for SVM-based response surface for structural reliability analysis. Probabilistic Engineering Mechanics, 41, 1–12.

37.   Bhattacharyya, B. (2023, March). On the use of sparse Bayesian learning-based polynomial chaos expansion for global reliability sensitivity analysis. Journal of Computational and Applied Mathematics, 420, 114819.

38.   Zhao, R., Creech, A., Borthwick, A. G. L., Venugopal, V., & Nishino, T. (2020). Aerodynamic Analysis of a Two-Bladed Vertical-Axis Wind Turbine Using a Coupled Unsteady RANS and Actuator Line Model. Energies, 13(4), 776–776.

39.   Chen, H., Birkelund, Y., Anfinsen, S. N., Staupe-Delgado, R., & Yuan, F. (2021). Assessing probabilistic modelling for wind speed from numerical weather prediction model and observation in the Arctic. Scientific reports, 11(1), 7613.